

Article

Function of a Deep-Buried Isolated Trench and Its Effect on Cracking Failure Characteristics of a Slope under Artificial Rainfall

Lei Wang ^{1,2} , Rongjian Li ^{1,*}, Shibin Zhang ¹ , Rongjin Li ^{3,4}, Weishi Bai ¹ and Huiping Xiao ⁵

¹ Institute of Geotechnical Engineering, Xi'an University of Technology, Xi'an 710048, China; wangl@yau.edu.cn (L.W.); zhangshbin@163.com (S.Z.); weishibai@126.com (W.B.)

² Architectural Engineering Institute, Yan'an University, Yan'an 716000, China

³ School of Management, Xi'an University of Architecture & Technology, Xi'an 710055, China; lirongjin12@126.com

⁴ Xi'an Jianchuang Geotechnique Technology Co., Ltd., Xi'an 710075, China

⁵ Huangshi City Construction Market Management Station, Huangshi 435000, China; 117629068716@163.com

* Correspondence: lirongjian@xaut.edu.cn; Tel.: +86-139-9129-8231

Abstract: When tests are conducted on the field slope under artificial rainfall, because artificial rainfall is often limited to implementation in the mode of local rainfall, there is a boundary constraint effect between the rainfall area and the non-rainfall area, which is manifested in the lateral infiltration of rainwater and the slope deformation retardation of non-rainfall area to the rainfall area. Firstly, a deep-buried isolated trench was proposed to solve these boundary constraints. Then, field cracking tests and the corresponding numerical simulation were conducted under rainfall. In the end, the response of water content and the cracking failure characteristics of the slope were analyzed during rainfall, and the effect of a deep-buried isolated trench on the cracking characteristics of the slope was evaluated. The results indicate that the proposed deep-buried isolated trench measure can effectively eliminate the deformation retardation resulting from the adjacent non-rainfall area so a through-crack parallel to the slope shoulder that extended on both sides of the boundary of the rainfall slope was observed at the slope crest and a cracking failure in the shape of the overall downward cutting was realized. As the crack occurred, the rainwater infiltration further aggravated expansion of depthwise cracks, and a local sliding zone was formed in the upper part of the slope. The deep-buried isolated trench solves the boundary constraints, such as lateral infiltration of rainwater and deformation retardation, and can provide an effective technical measure for the field slope test under artificial rainfall.

Keywords: artificial rainfall; loess slope; field test; deep-buried isolated trench; cracking failure characteristics



Citation: Wang, L.; Li, R.; Zhang, S.; Li, R.; Bai, W.; Xiao, H. Function of a Deep-Buried Isolated Trench and Its Effect on Cracking Failure Characteristics of a Slope under Artificial Rainfall. *Water* **2022**, *14*, 1123. <https://doi.org/10.3390/w14071123>

Academic Editors: Xingwei Ren, Zili Dai and Fangzhou Liu

Received: 18 February 2022

Accepted: 30 March 2022

Published: 31 March 2022

Publisher's Note: MDPI stays neutral with regard to jurisdictional claims in published maps and institutional affiliations.



Copyright: © 2022 by the authors. Licensee MDPI, Basel, Switzerland. This article is an open access article distributed under the terms and conditions of the Creative Commons Attribution (CC BY) license (<https://creativecommons.org/licenses/by/4.0/>).

1. Introduction

Landslides occur frequently in the Chinese Loess Plateau, which threatens people's daily lives and production safety. Rainfall is a vital inducer of landslides [1]. Rainy weather, especially continuous intensive rainfall, easily causes large-scale landslides [2,3]. Therefore, it is a very important to study the mechanism of rainfall-induced landslide disasters. When studying the impact of rainfall on slope damage, researchers often pay more attention to the response of various parameters of the slope while ignoring the importance of boundary conditions. Whether scientific research is carried out through experiments or numerical simulation, the boundary conditions are the key factors that affect the test results, that is, the results will be more accurate only by setting reasonable boundary conditions.

The boundary conditions of a landslide play a decisive role in its failure mode and characteristics. Researchers studied typical loess landslides in northwest China and Heifangtai landslides in Gansu Province, China [4,5]. The results demonstrated that the landslides are in the form of a round-backed chair [6]; in other words, the upper edge of the natural

landslides generally moves downward on both sides. Moreover, a natural landslide is characterized by more severe damage near the central axis along the longitudinal direction, with weakening damage toward the flanks. Such uneven failure is obviously caused by boundary constraints. The soil near the central axis is minimally affected by boundary constraints, whereas the left and right edges are more significantly affected. As we all know, the theory of material mechanics, based on the stress characteristics of slopes, assumes that the slope is in plane strain. Thus, in a slope collapse or landslide disaster, the form of deformation and failure should be in the shape of overall downward cutting. However, the phenomenon of natural landslides is unlike that of an idealized form, with the constraints at the rainfall boundary.

Several studies have been conducted using a simulation numerical method to analyze the influence of lateral boundary conditions on the model. Griffiths et al. [7] set the boundary conditions as 'rough-smooth' and 'rough-rough' for the analysis of slope stability; however, the failure form of the slope was not mentioned in their paper. Ashraf et al. [8] constructed a core of low-permeability soil on both sides to realize different hydraulic conductivities between the center and the two sides of seepage flow. However, to apply such a method to numerical simulation of slope engineering, innovative exploration is needed. Hou et al. [9] introduced an interface film element to the air element method in order to improve the poor imitation occurring on the contact surface between strong and weak permeable media. However, for different engineering problems, the relative permeability coefficient of the interface film element needs further study.

Therefore, when studying a specific failure mechanism of the rainfall slope, in order to obtain reasonable rainfall infiltration data of the field slope, controllable artificial rainfall is the preferred rainfall mode. Responses of various parameters can be monitored through field slope tests in local slope under artificial rainfall [10]. The advantages of conducting on-site rainfall tests are significant, but at the same time, due to the limited width of the test slope and the constraint boundary, it is difficult to realize the idealized failure mode in a field rainfall test.

To reduce the adverse effect of boundary constraints and lateral infiltration, scholars have taken some measures in field tests under local artificial rainfall, such as metal plates measuring 200 mm high and buried about 80 mm into the slope to prevent runoff to other areas [11]. A piece of hard white iron sheet with a height of 60 cm was buried in the soil at the boundary of the rainfall area, called a rigid isolation measure [12]. The rigid isolation measure was also applied by Zhou et al. [13,14] in a field test in which the buried depth was 50 cm. In view of the insufficient buried depth in rigid isolation measure, Fu et al. [15] buried a hard white iron sheet with a height of 1.5 m into the soil at the rainfall boundary.

In the previous tests, the rigid isolation measure was widely used at the boundary of the rainfall area, but there were three defects that need to be addressed. Firstly, the flattened layout of this kind of hard material is difficult in construction. Secondly, due to the hard properties of the material, it cannot be buried more than 1.5 m in construction, although the infiltration depth of rainwater can reach 3.0 m in the loess area [16]. Apparently, the measure hardly prevented lateral loss at the deeper depth. Thirdly, the surface of the material is not quite smooth, so the uneven deformation will be aggravated again in the process of expansion. The rough surface increases friction between soil and the material. As a result, the free deformation of the rainfall area is hindered by the deformation of the non-rainfall area.

In summary, when a failure test is conducted on a field slope under local artificial rainfall, the methods used to improve boundary constraints, such as the rigid isolation method, have adverse effects on the test results. In view of the above deficiencies, a deep-buried isolated trench at the rainfall boundary was proposed to solve these boundary constraints. Then, field tests and the corresponding numerical simulation were conducted under rainfall, and the response of water content and the cracking failure characteristics of the slope were analyzed. In the end, the effect of a deep-buried isolated trench on cracking characteristics was evaluated. The purpose of this study was to eliminate the constraint at

the rainfall boundary under local artificial rainfall and to realize the failure mode of overall downward cutting. Overall, this study provides an effective technical measure for the field slope test under artificial rainfall.

2. Methods and Materials

2.1. Deep-Buried Isolated Trench Method

When the artificial rainfall test is conducted on a local slope, because the width of the rainfall region is limited, there is a boundary constraint effect between the rainfall area and the non-rainfall area. The effect is manifested in the lateral infiltration and dissipation of rainwater, as well as the slope deformation retardation of the non-rainfall area to the rainfall area. Thus, the infiltration response will be weakened, and the cracking failure form of the slope will inevitably be affected.

In order to solve these boundary constraints and problems under local artificial rainfall, we proposed a measure termed deep-buried isolated trench. The deep-buried isolated trench measure was implemented three steps, as follows:

- (1) We selected the natural slope with soil quality and slope that met the test requirements. A trench with a width of 0.1 m on both sides of the boundary close to the rainfall region was vertically excavated downward along the slope crest and surface to the specified depth. The depth of the trench was greater than the maximum local statistic value of the infiltration depth. The trench was maintained upright, and the side wall was flat during excavation. The floating soil at the bottom was finally cleaned up to ensure that it did not influence the effect of the isolated trench.
- (2) We calculated the required area of the whole isolated cloth according to the depth and width of the trench. Afterward, the isolated cloth, with the characteristics of a dense texture, softness, good ductility, impermeability, and a smooth surface was cut out and spread out on the ground and was slowly placed at the bottom of the trench to fully cover the side wall of the trench.
- (3) We backfilled the trench layer by layer and tamped after every 0.2 m of soil thickness to achieve a compactness close to that of the original slope. The slope crest surface of the isolated trench was leveled.
- (4) A schematic of the proposed deep-buried isolated trench of the field slope is shown in Figure 1a, and the slope after construction with the isolated trench is shown in Figure 1b.

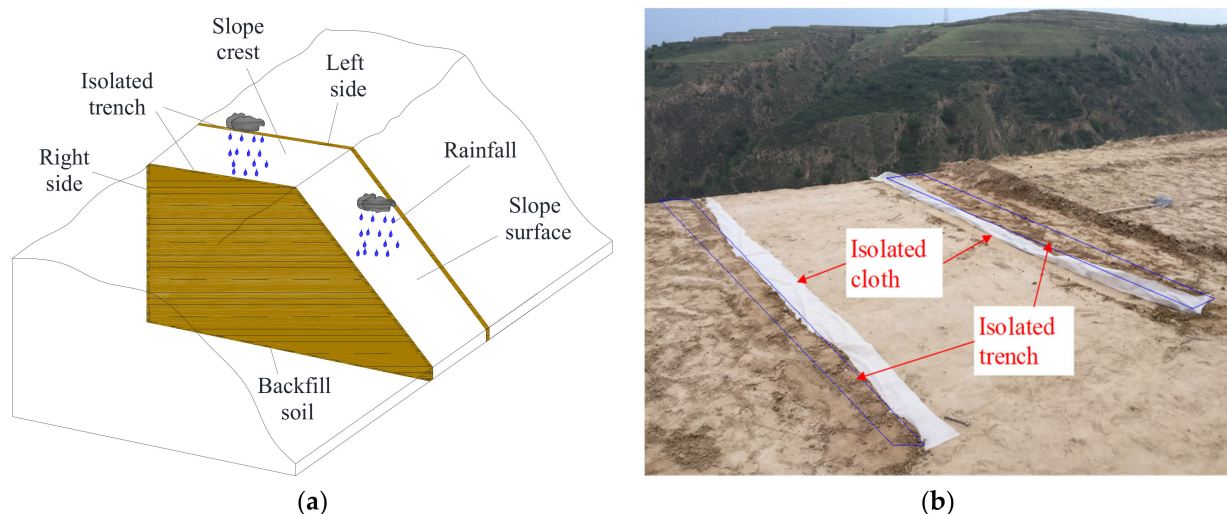


Figure 1. Treatment measure of deep-buried isolated trench. (a) Schematic diagram of the isolated trench; (b) the slope crest after construction with isolated trench.

The proposed measure has a solid theoretical foundation and some advantages for practice implementation as follows:

- (1) The deep-buried isolated trench can effectively prevent the lateral loss of rainwater that infiltrates into deep within the rainfall area by means of the impermeable isolated cloth, so as to separate the rainfall area from the non-rainfall region, and an independent rainfall area can be formed in a better test condition.
- (2) In order to eliminate retardation deformation in the rainfall area resulting from the boundary constraint of the adjacent non-rainfall area, an isolated cloth with smooth surface and lower friction coefficient is used in the deep-buried isolated trench. The approach ensures the natural deformation and the crack from initiation to expansion in rainfall area. Thus, the free deformation of the soil will be realized in the test slope.
- (3) The isolated trench is leveled and backfilled layer by layer so that the stress of the rainfall area of the field slope is consistent with that of the non-rain area, and the plane strain stress state will be restored. In short, an overall downward-cutting form of the failure can be achieved, and the accuracy and reliability of the test slope can be improved under local artificial rainfall.

2.2. Basic Information of Test Slope

Wuqi County is located in the hilly and gully region of the hinterland of the Loess Plateau, about 150 km west of Yan'an City. There is mainly large-grained silty loess with strong collapsibility in this region. The average annual precipitation is 450 mm; however, the rainfall is concentrated from July to September, reaching about 65% of the annual precipitation and frequently inducing landslide disasters.

A sloping ground with a height of 5 m was selected as the site in Wugu Town, Wuqi Count. The soil is homogeneous within 5 m below the surface and is brownish-yellow with a large particle size. The viscosity is not strong, composed of silty loess. Before the test, the weeds on the slope surface were cleaned up. Two slopes with a width 3 m and an inclination of 60° were formed. The natural slope is shown in Figure 2a, and the trimmed slope is shown in Figure 2b. Physical and mechanical parameters were measured by undisturbed soil samples, as shown in Table 1.



Figure 2. Test slope: (a) natural slope, (b) test slope after trimming.

Table 1. Physical and mechanical characteristics of loess.

Natural Water Content (%)	Natural Density ($\text{g}\cdot\text{cm}^{-3}$)	Liquid Limit (%)	Plastic Limit (%)	Permeability Coefficient ($\text{m}\cdot\text{s}^{-1}$)	Collapsibility Coefficient	Cohesion (kPa)		Internal Friction Angle ($^{\circ}$)	
8.93	1.44	26.43	16.42	5.72×10^{-6}	0.11	Natural 16.32	Saturation 9.05	Natural 26.62	Saturation 23.93

2.3. Construction of Deep-Buried Isolated Trench

The width of rainfall range is 2.5 m, and the height is 5 m, so the ratio of width to height is 0.5. In addition, polyethylene plastic cloth with characteristics including a dense texture, softness, good ductility, impermeability, and a smooth surface, was selected as the isolated cloth finally. Because the infiltration depth in the rainfall region can reach 3.0 m [17], in order to prevent lateral seepage loss of rainwater from affecting the test results, a trench with a width of 0.1 m and a depth 4 m was excavated at the boundary outside the rainfall area (Figure 3a), laid with isolated cloth (Figure 3b), backfilled and compacted in layers (Figure 3c), and covered for protection (Figure 3d).

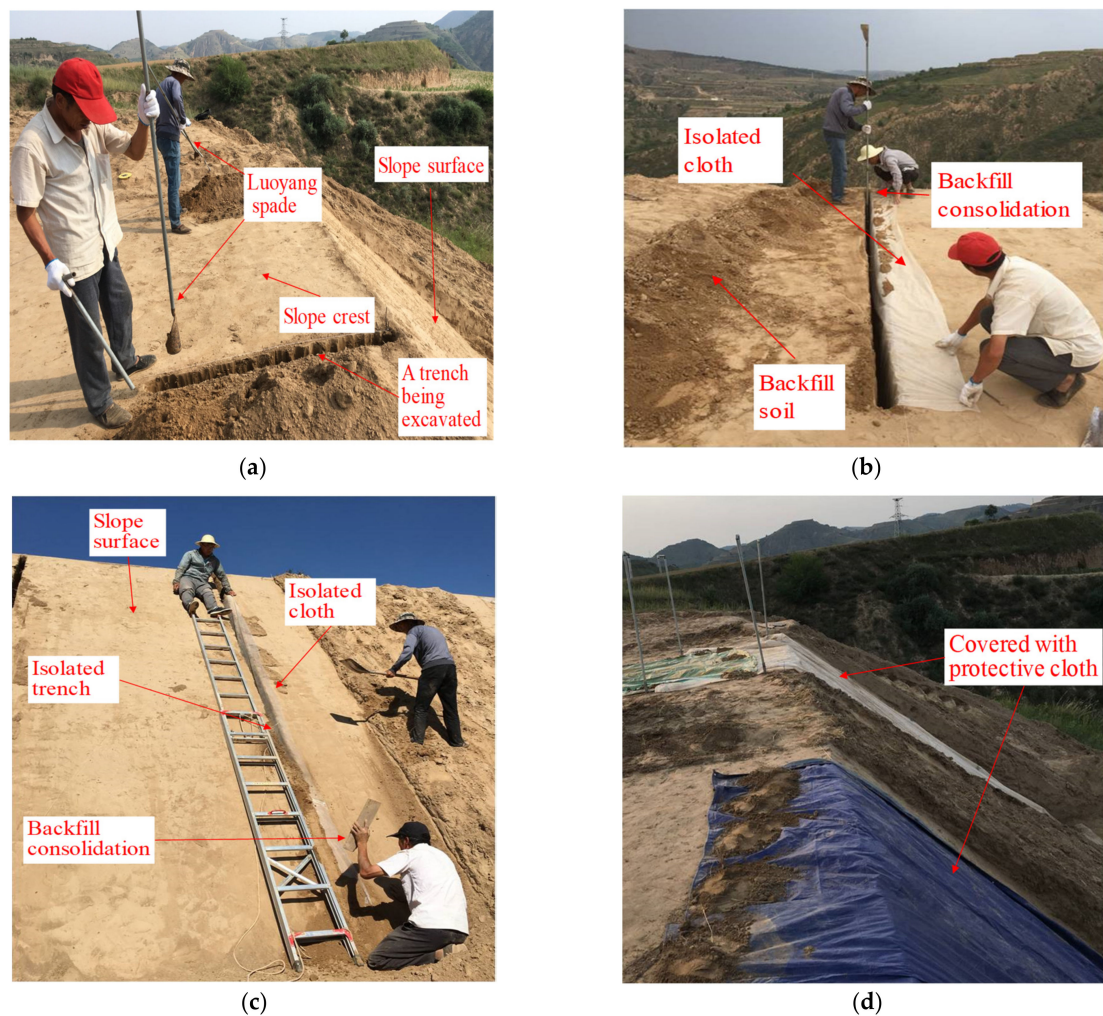


Figure 3. Construction process of isolated trench: (a) excavation of isolated trench; (b) laying isolated cloth and backfill soil at the slope crest; (c) laying isolated cloth and backfill soil at the slope surface; (d) protection after construction.

2.4. Embedding of Monitoring Equipment

Based on the characteristics of distribution and prominent disasters induced by rainfall in this region [1,2,17], the test was conducted on slope 1 under heavy rainfall with a rainfall intensity of 57 mm in 24 h, whereas on slope 2, the test was conducted under a rainstorm with a rainfall intensity of 87 mm in 24 h and a duration of continuous rainfall of 144 h. To measure the data of volumetric water content, six moisture sensors (No. E₁–E₆) were embedded in each slope. Then, the impact was analyzed on the seepage field of the slope. A diagram of the sensor layout is shown in Figure 4. A picture of local artificial rainfall on the slope crest is shown in Figure 5a, and that of on the slope surface is shown in Figure 5b.

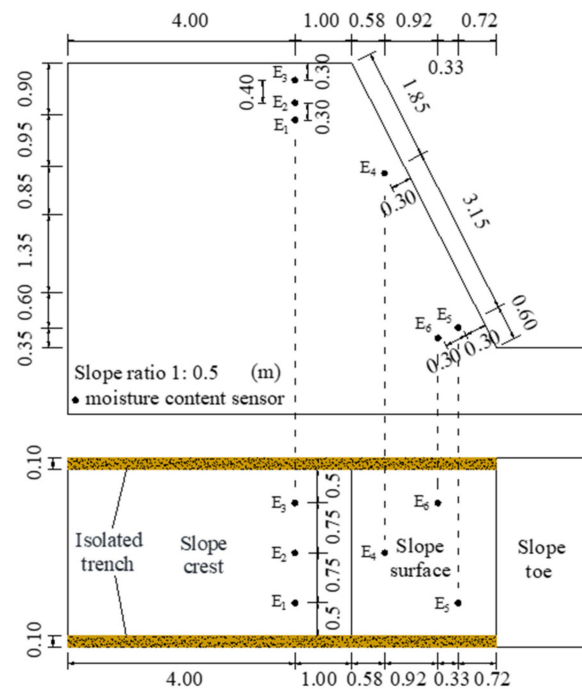


Figure 4. Schematic diagram of moisture sensor layout.

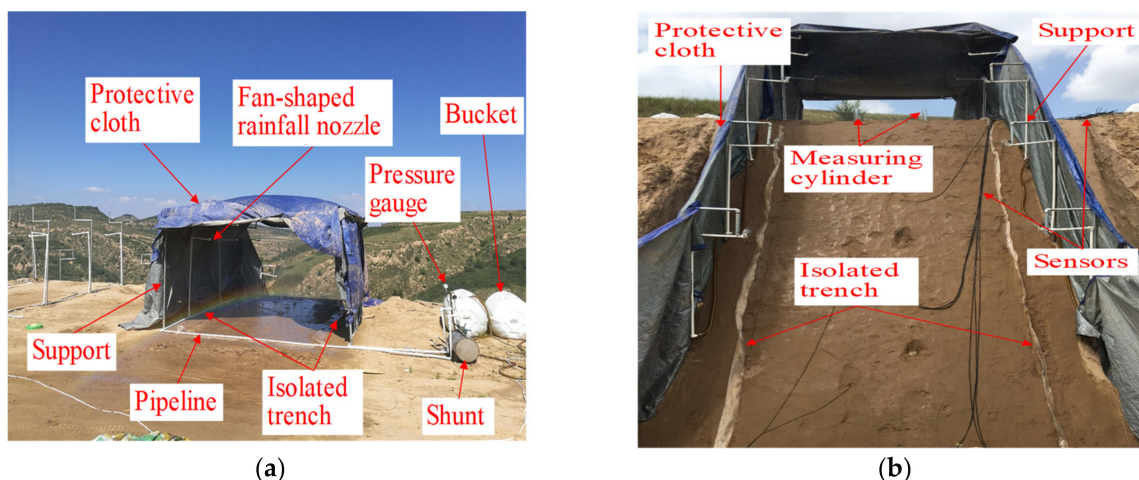


Figure 5. Rainfall on test site: (a) rainfall on the slope crest; (b) rainfall on the slope surface.

3. Results

3.1. Characteristics of Cracking and Failure of Test Slopes

Rainwater infiltration was accompanied by a gradual deformation and displacement under local artificial rainfall. It was mainly manifested in the development of a through-crack parallel to the slope shoulder. The through-crack extended to both sides of the

boundary at the slope crest 50–60 cm away from the slope shoulder during heavy rainfall and rainstorm, as shown in Figure 6a,b and Figure 7a,b. The deformation and displacement resulted in a differential settlement and a region of bulging and collapse on the slope surface under heavy rainfall and in rainstorm, as shown in Figures 6c and 7c, respectively.

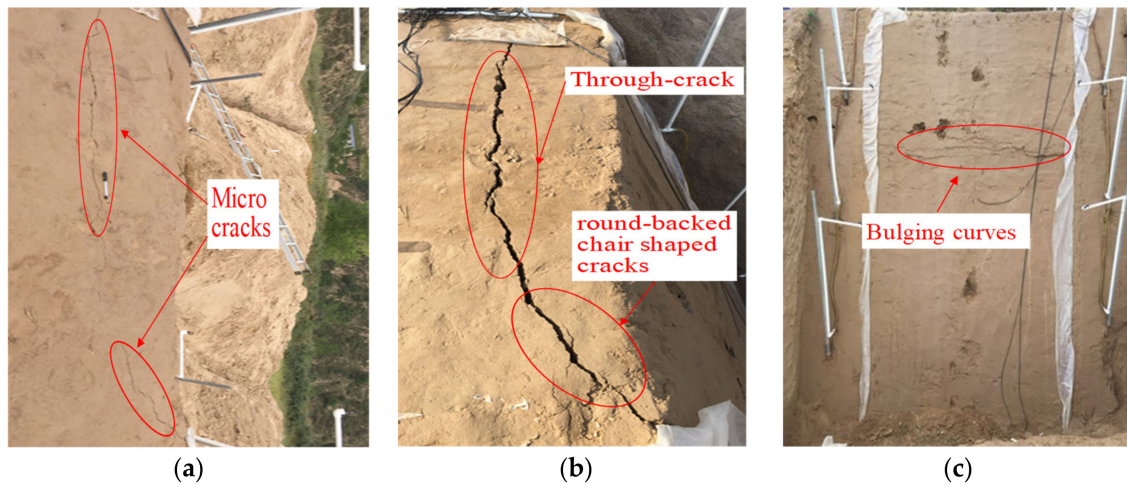


Figure 6. Cracks of the slope under heavy rainfall: (a) microcrack growth; (b) transverse penetration of crack at the slope crest; (c) bulging curves at the slope surface.

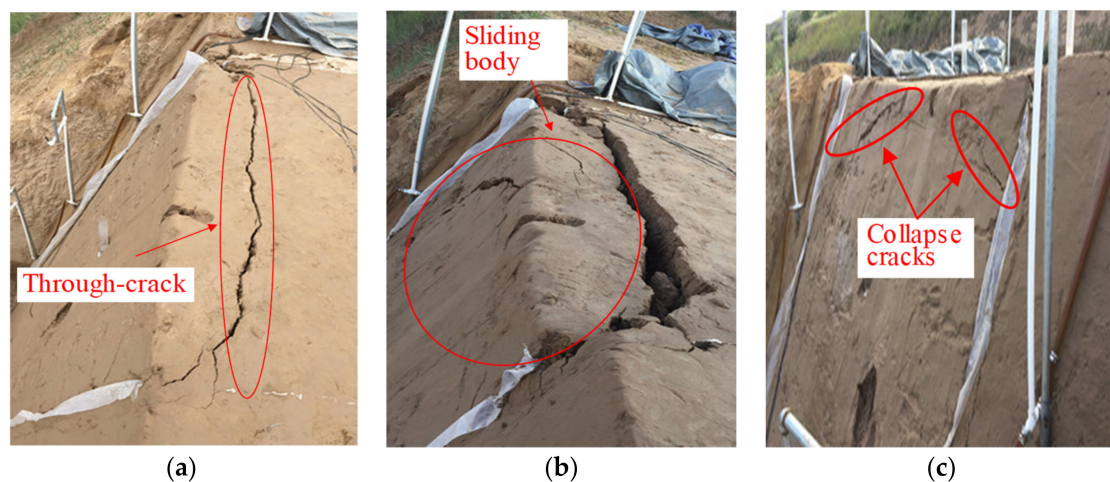


Figure 7. Cracking of the slope under rainstorm: (a) through-crack at the slope crest; (b) sliding body of the slope; (c) collapse cracks at the slope surface.

3.2. Cracking and Failure Process of the Test Slopes

Numerous engineering practices have shown that slopes become unstable because of cracking and deformation caused by rainfall [18,19]. Once cracks appear at the slope crest, safety becomes more difficult to guarantee [20]. In addition, Zhang et al. [12] reported that cracks are the key inducers of landslides. Therefore, in this test, the inducement and characteristics of cracking and failure were observed during rainfall. The process of rainfall cracking and failure can be divided into four stages: slope shoulder gully, crack development at the slope crest, crack propagation and slope bulging, and crack penetration and slope collapse.

In the first stage, a rill was formed on the shoulder of the slope. The surface of the slope crest was flat before rainfall, but the splashing action of raindrops caused the surface to become uneven immediately after the rainfall started. Thus, as the rainwater further eroded the soil, a microflow was gradually developed, generating vertical and horizontal micro runoff. Consequently, a crisscross micro rill was formed on the slope crest. The ponding

area of the local surface gradually expanded to a continuous flow to the slope surface, and the scouring action had a traction effect on the surface during longitudinal runoff; the surface loess was eroded to form an apparent rill with a significant effect on the slope crest. The test results demonstrated that there are three important prerequisites for cracks at the slope crest, mainly including the progressive gully effect of erosion, the scouring caused by rainfall, as well as the advantage of the free surface at the front edge of the slope.

In the second stage, cracks were developed at the slope crest. With the continuous infiltration of rainwater, the soil at the slope crest was close to saturation. Therefore, if no tensile strength exists between soil particles, the soil can undergo tensile cracking. Moreover, the tensile strength between the soil particles, which was originally very low, will decrease rapidly to zero. The main factors are the influence of the free surface of the slope and the weakening effect of rainwater infiltration. Thus, the tensioned microcracks occurred at the surface of the slope crest as soon as tensile strength of the loess was reduced or even completely lost.

In the third stage, crack propagation and slope bulging occurred. At the initial stage of crack formation, only a small amount of rainwater infiltrated into the crack. Part of the remaining rainwater continued to infiltrate, whereas the other part was discharged by surface runoff, which caused serious scouring on the slope surface. With an increase in water infiltration depth, the soil along the crack surface was destroyed gradually, whereas the tensile strength of deep loess was greatly reduced. The structure composed of soil particles near the crack surface was also destroyed by soaking because the area near the crack was always saturated, and the cementation between soil particles was reduced. These behaviors resulted in a significant reduction in soil cohesion. In addition, the cracks gradually evolved into seepage channels of rainwater as the vertical cracks extended [21]. The pressure between the top and the bottom of the crack, difference, and the erosion of water on the side wall facilitated the crack expansion [22]. A structural plane was ultimately formed inside the slope. Thus, an independent soil column was formed by the front edge of the crack. Under the influence of factors such as seepage pressure and collapsibility of soil, the independent soil column had obvious settlement deformation, and the front and rear edges of cracks formed a downward-cutting displacement. Moreover, multiple bulging cracks appeared on the slope surface, and a bulging zone was formed between the shear outlet and the slope shoulder.

In the fourth stage, crack penetration and slope collapse occurred. The weight of the soil, with a certain thickness below the slope crest, increased substantially as the rainfall continued. In addition, rainwater infiltration led to a considerable reduction in the shear strength of the soil, resulting in failure at the bottom of the crack. The crack extended along the oblique direction and formed a shear outlet at the slope surface under the swelling area. At this time, the crack at the crest extended to the slope surface. The slope evolved into a sliding body of the landslide, with the accumulation of settlement of the independent soil column at the front cracks, as well as the development of lateral displacement toward the free surface of the front edge. The rainfall-induced cracking at the slope crest finally evolved into a landslide. The cracking and failure form of cohesive soil in this test is considerably different from that of cohesionless soil. In rainfall tests of slopes in cohesionless soil, tension cracks always gradually develop upward from the slope toe [23].

4. Discussion

4.1. Analysis of the Change Law of Volumetric Water Content in Monitoring Points

During the local artificial rainfall on the test slope, we collected volumetric water content data of measuring points at different depths and positions. The changes in volumetric water content of the measuring points are shown in Figure 8. The change law of slope 1 under heavy rainfall is shown in Figure 8a, whereas that of slope 2 under a rainstorm is shown in Figure 8b.

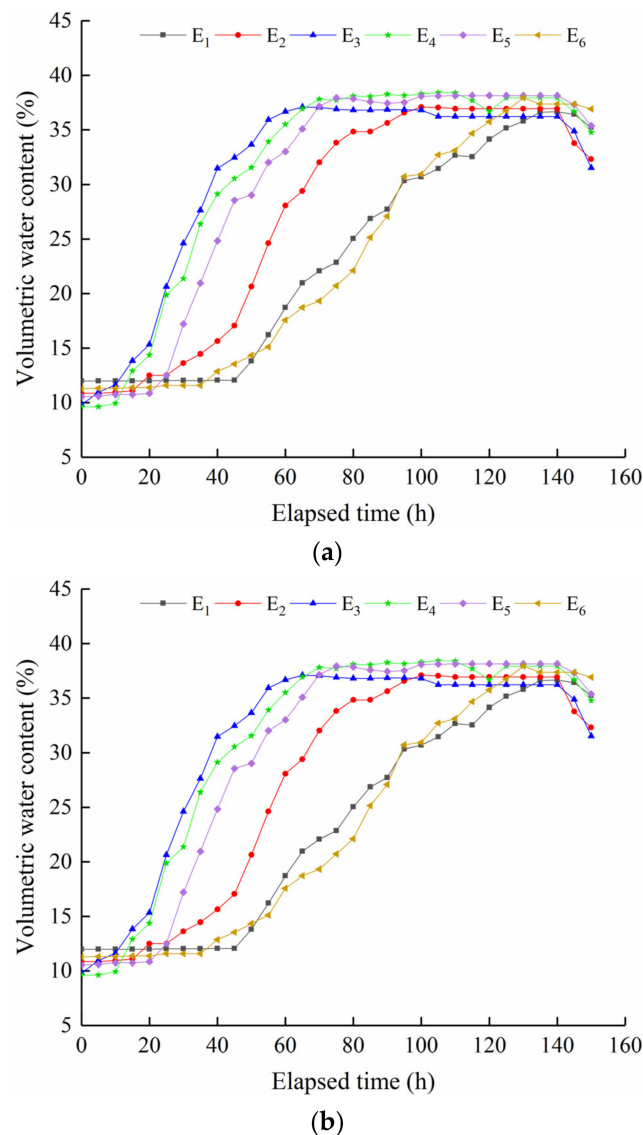


Figure 8. Change curves of volumetric water content at measuring points: (a) under heavy rainfall; (b) under rainstorm.

By comparing Figure 8a,b, on the one hand, the average gradient of the change rules is small in slope 1, i.e., the initial growth time of volumetric water content is scattered in slope 1, whereas that of in slope 2 is relatively concentrated. On the other hand, the greater the rainfall intensity, the faster the infiltration rate of rainwater in the silty loess slope. In addition, it can be observed that the initial growth time of E_1 is approximately 10 h later than that of E_6 in slope 1, whereas in slope 2, the initial growth time of E_1 is approximately 5 h earlier than that of E_6 . This phenomenon is considerably different from the infiltration law in the conventional slope [24] and causes the difference in deformation, as discussed in detail in Section 4.3.

4.2. Analysis of Cracking Change Law on Slope Crest

Microcracks appeared at the slope crest when heavy rainfall lasted for 84 h (Figure 6a), developing into cracks with a depth of approximately 55 cm and a width of approximately 3 cm when the rainfall continued for 132 h in slope 1 (Figure 6b). Microcracks occurred at the slope crest when the rainstorm lasted for 76 h, developing into a crack with a depth of 60 cm and a width of 3 cm when the rainstorm lasted for 122 h in slope 2 (Figure 7a). It is worth noting that the initial cracking time in slope 1 is slightly later than that in slope 2.

Based on the data of cracking width measured during rainfall, the curves of crack width with time at the crest of slope 1 and slope 2 are shown in Figure 9. The crack width increased with local artificial rainfall, which is shown as a pattern of alternating growth. At the initial stage of cracking, the rainwater and depth of infiltration were limited [25], resulting in the slow growth of the crack width. However, the rapidly increase in rainwater infiltration depth at the later stage resulted in a substantial increase in the weight of the soil, thus accelerating crack expansion. In addition, at the later stage of rainfall, the growth of crack width was considerably facilitated by the scouring of large-scale runoff caused by the rainstorm [26].

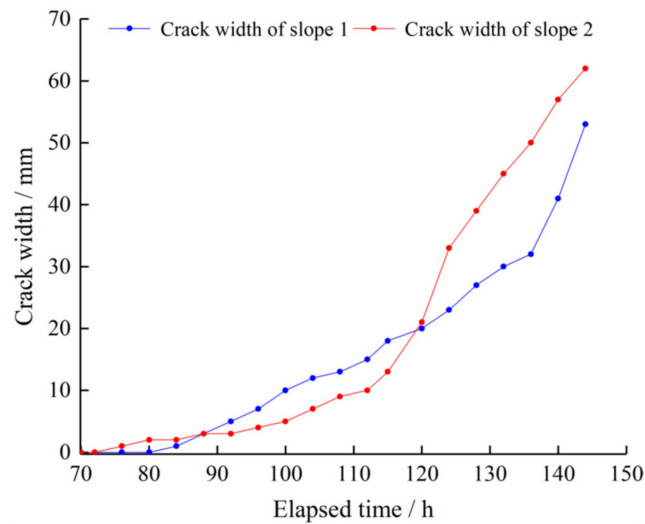


Figure 9. Curves of crack width with time in test slopes.

4.3. Evaluation of Cracking Failure Characteristics with Deep-Buried Isolated Trench

Two schematic diagrams of cracking and deformation on the test slopes under local artificial rainfall are shown in Figure 10; in particular, that under heavy rainfall is shown in Figure 10a, whereas that under rainstorm is shown in Figure 10b. It can be observed that a series of transverse microcracks were generated on the lower part of the local sliding body of slope 1, whereas some collapse cracks were formed on the local sliding body of slope 2. These observations indicate that the deformation on the surface of the loess slope under rainstorm was more severe than that under heavy rainfall. The results also demonstrate that the distance between the slope shear outlet and the slope shoulder under rainstorm were greater than those under heavy rainfall. When the soil of the superficial layer tended to be saturated, large-scale runoff formed on the surface of the steep slope under the rainstorm, and its scouring effect on the slope surface was more significant.

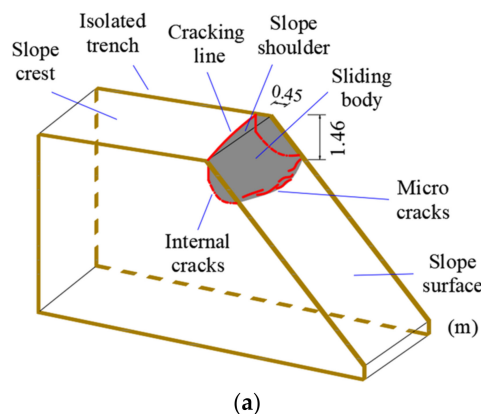


Figure 10. Cont.

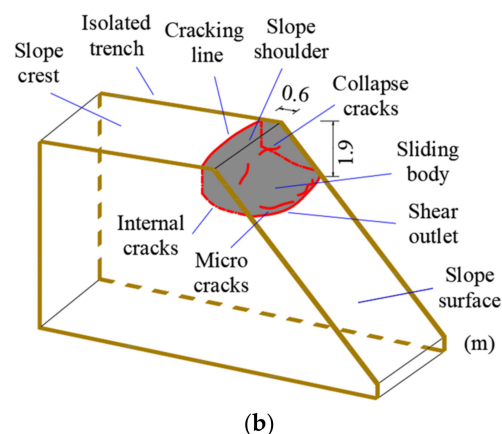


Figure 10. Schematic diagram of failure mode under rainfall of the local slope: (a) heavy rainfall, (b) rainstorm.

A crack was observed in the shape of a round-backed curve, extending from the left boundary to the right edge at the crest of slope 1, whereas a through-crack parallel to the slope shoulder extending to both boundaries of the rainfall slope was observed at the slope crest of slope 2.

When the isolated trench was backfilled, the soil compaction was higher because of excessive tamps at the right boundary of slope 1, resulting in a compaction effect on the adjacent soil and uneven compactness in the transverse direction, which may have caused a significant reduction in permeability according to the different degree of compaction [27]. Therefore, the rate of rainwater infiltration was reduced, and it took a longer time for rainwater to infiltrate into measuring point E_1 in slope 1. Moreover, the greater horizontal pressure led to an increased friction between the isolated cloth and the soil. Under the action of the above factors, a crack in the shape of a round-backed curve occurred and extended from the left boundary to the right edge at the crest of slope 1. This crack mode completely corresponded to the abnormal phenomenon, i.e., that the initial growth time of measuring point E_1 was approximately 10 h later than that of measuring point E_6 in slope 1. The abnormal phenomenon was caused by the uneven compaction of backfill soil in the isolated trench on both boundaries.

Under the uniform compaction of the backfill soil in the isolated trench on both boundaries, the through-crack parallel to the slope shoulder developed at the slope crest in slope 2 showed that the constraint at the rainfall boundary was almost eliminated by means of the deep-buried isolated trench. In other words, when the isolated trench measure was implemented, the cracking failure form was close to the overall downward cutting of the slope, which may simulate some phenomena, consistent with the most damaged area near the central axis and reports of landslides in [4,5]. The mode of a through-crack parallel to the slope shoulder demonstrated that the proposed deep-buried isolated trench measure can effectively eliminate deformation retardation outside the rainfall range, and then the overall downward-cutting cracking form was realized. Thus, the deep-buried isolated trench measure is proven to provide more guarantee of the boundary conditions.

4.4. Numerical Simulation Analysis of Rainfall Slope in Double Isolated Trench

4.4.1. Model Establishment and Boundary Condition

By adopting the isolated trench measure, the test results showed that the cracking forms are all approximately through-cracks parallel to the slope shoulder. In order to evaluate the harm of slope cracks, some research has been conducted on slope cracking and deformation caused by simulated rainfall [28–30]. Hence, Geo-Studio [31] finite-element software was used to establish two kinds of numerical models under plane strain. One numerical model (NMOD) was used to simulate continuous rainfall infiltration without cracks, and the other numerical model (NMODC) was used to simulate continuous

rainfall infiltration under activation cracks. The crack had a depth of 60 cm and a width of 3 cm. The crack was activated when the simulated rainstorm lasted for 122 h, so as to conform to the characteristics of cracking failure in test slope 2. The simulated rainfall parameters in numerical simulation analysis are consistent with those used in the field test.

The site of the artificial rainfall test was at the top of the mountain, and the groundwater level was very deep. Through numerical experiments, the groundwater level was set at 10 m below the slope bottom in the numerical model. The numerical model and the monitoring points in the numerical simulation are shown in Figure 11.

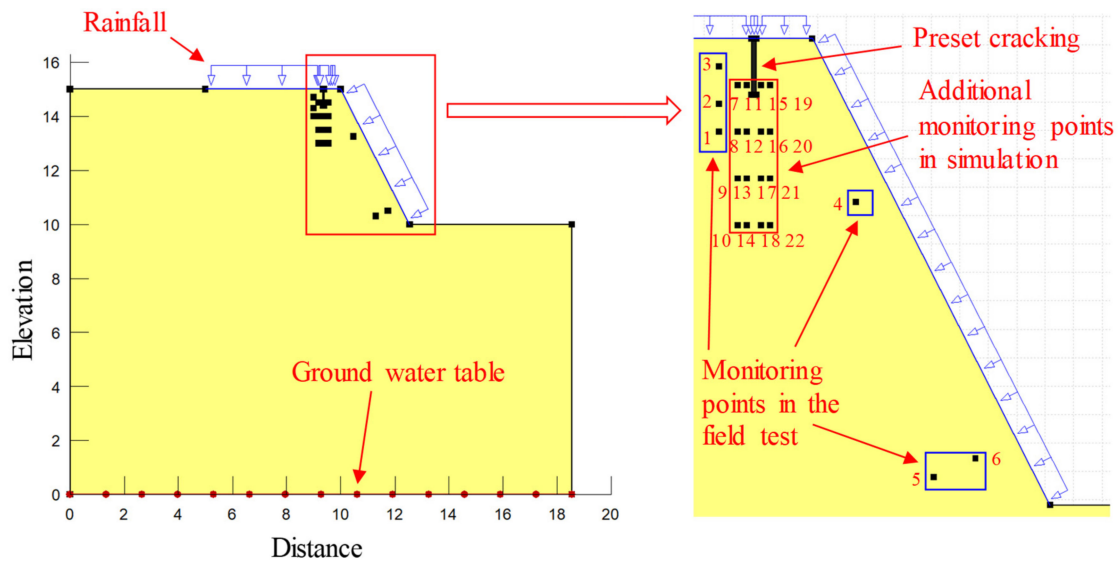


Figure 11. Monitoring points of numerical models under simulated rainstorm.

In order to compare with the test results, the six monitoring points (N_{n1} – N_{n6} represent the monitoring points in NMOD and N_{y1} – N_{y6} represent the monitoring points in NMODC) were established in the two numerical models, the six monitoring points were set, and the location of the monitoring points was the same as that of the field slope. Moreover, in order to contrastively analyze the influence of cracks on infiltration, 16 monitoring points (N_{n7} – N_{n22} in NMOD and N_{y7} – N_{y22} in NMODC) were arranged in layers in the two numerical models, with a monitoring time of 240 h.

The most significant feature of test slope 2 was the formation of a through-crack on the slope crest. Therefore, features of cracks must be fully considered in analysis of numerical simulations, particularly for cracks with the same characteristics as those in the field test, such as crack position, depth, and parameters of infiltration [32]. Consideration of these features enables an accurate analysis in the numerical model.

Elahe et al. [33] simulated slope cracks by weakening properties of material and found that surface cracking had a considerable impact on slope safety. Based on the cracking failure process under artificial rainfall observed in this study, the geometric parameters of the crack in NMODC were set as a depth of 60 cm and a width of 3 cm when the simulated rainstorm lasted for 122 h. In this study, we applied the method of equivalent permeability coefficient [34] to accurately determine the crack characteristics. According to this method, the crack area was accurately simulated by changing the value of material parameters, and the continuation of crack was ignored. The soil in the crack zone in NMODC, with the same position as the crack zone of test slope 2, was set as a large permeability coefficient. The soil gravity in the crack zone was set as zero from 122 h to 240 h.

The physical parameters of the two numerical models are shown in Table 2. To accurately analyze the change rule of unsaturated soil seepage during simulated rainfall,

the V-G model of unsaturated soil [35] was selected to obtain values of the parameters. The formula is given as:

$$\theta_w = \theta_r + \frac{\theta_s - \theta_r}{[1 + (\psi/a)^n]^m} \tag{1}$$

$$k_w = k_s \frac{[1 - a\psi^{n-1}(1 + (a\psi^n)^{-m})]^2}{(1 + a\psi^n)^{m/2}} \tag{2}$$

where θ_r is the saturated water content; θ_s is the residual water content; ψ is the negative pore water pressure; a , n , and m are the fitting parameters; and k_s is the saturated permeability coefficient. The k_s of the soil in the crack zone was 0.5 m/s and 5.72×10^{-6} m/s in the other zone.

Table 2. Mechanical properties of slope material.

Material	$\theta_r/\%$	$\theta_s/\%$	a/kPa	n	m	$k_s/\text{m}\cdot\text{s}^{-1}$
Soil	38.4	2.7	12.92	1.68	0.38	5.72×10^{-6}

4.4.2. Discussion on Change Law of Volumetric Water Content in Monitoring Points

Figure 12 displays the change curves of volumetric water content, including the monitoring points of N_{n1} – N_{n6} in NMOD and N_{y1} – N_{y6} in NMODC. We observed that the volumetric water content in the two numerical models was different, as the crack was set at 122 h of simulated rainfall.

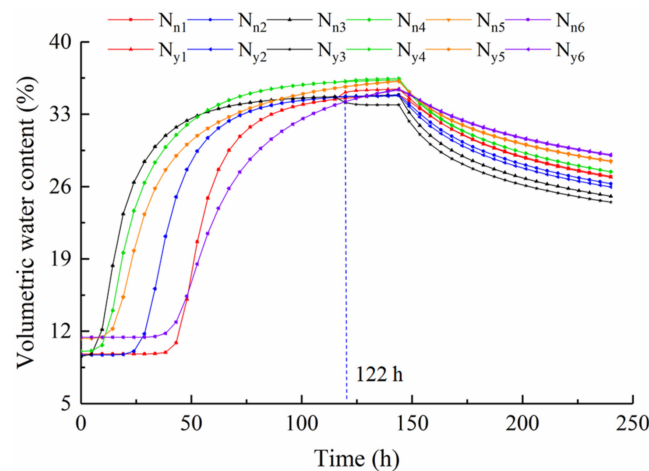


Figure 12. Change curves of volumetric water content in the two numerical simulations.

The change trend (Figure 12) of volumetric water content at N_{y1} – N_{y6} in NMODC under simulated rainstorm was largely consistent with that in the field test results (Figure 10b). This indicates that the seepage field after applying the isolated trench was largely consistent with that of the numerical model (NMODC). In addition, the volumetric water content in the test slope decreased faster than that in NMODC when the simulated rainfall stopped. This phenomenon occurred because a crack with fixed geometric parameters was set in NMODC, whereas the crack expanded further in the field test, even after the simulated rainfall was over.

In particular, the volumetric water content of N_{n3} in NMOD and N_{y3} in NMODC, which were closest to the slope crest, varied considerably after activation of the crack in NMODC. The volumetric water content of N_{y3} in NMODC was less than that of N_{n3} in NMOD because N_{y3} was close to the preset crack. The lateral infiltration of simulated rainwater led to a change in water content at N_{y3} . As the measuring points were far away from the crack in NMODC, the variation law of the volumetric water content was close to that in NMOD.

In addition, the 16 numerical monitoring points in NMOD and in NMODC were distributed in the four layers. They were divided into upper, middle, lower, and bottom monitoring points. The change curves of volumetric water content from 100 h after the beginning of simulated rainfall are shown in Figure 13a–d.

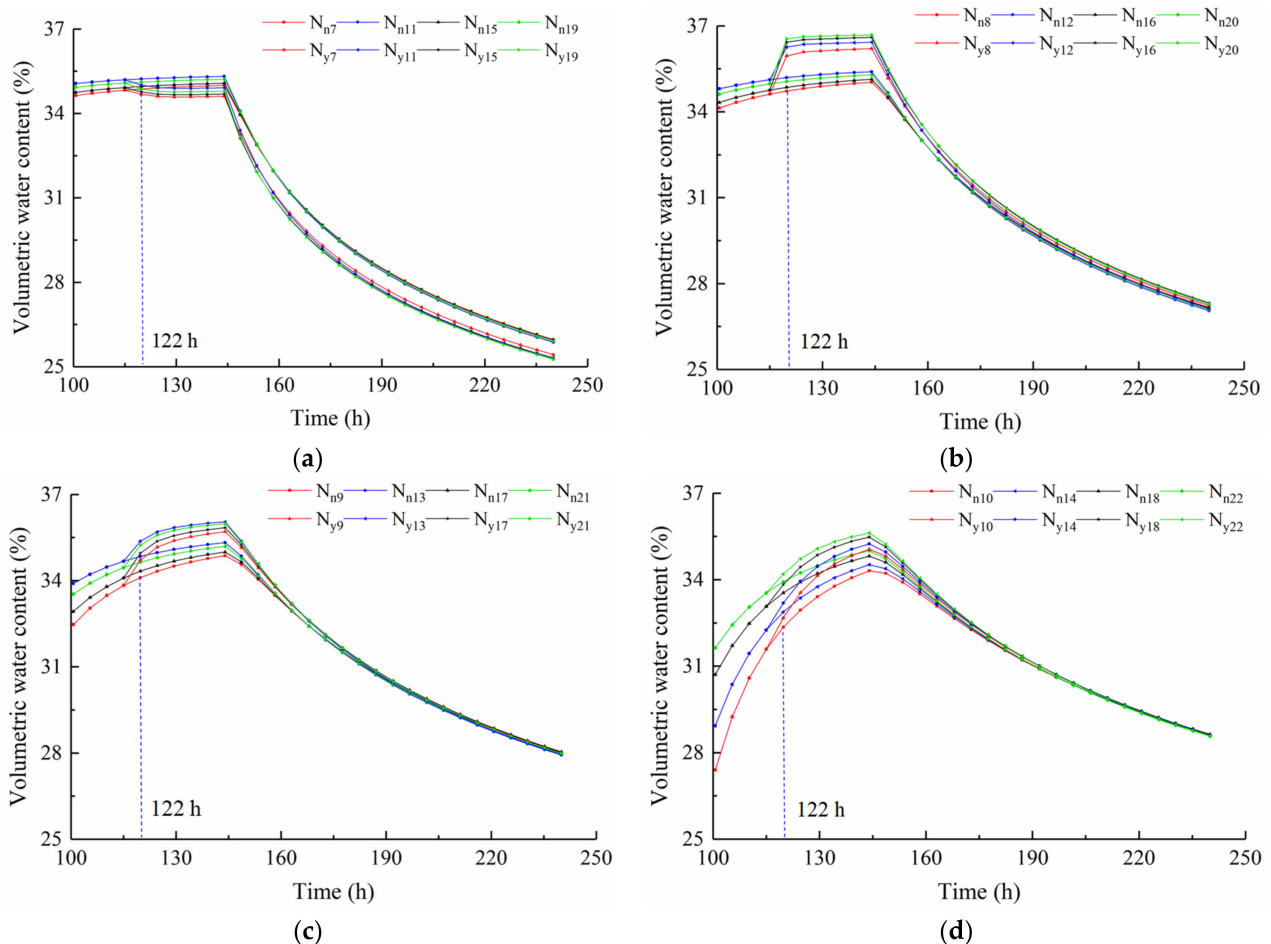


Figure 13. Curves of volumetric water content in additional monitoring points in the two numerical simulations: (a) upper points; (b) middle points; (c) lower points; (d) bottom points.

According to the upper numerical monitoring points, the variation rule of volumetric water content of points (N_{n7} , N_{n11} , N_{n15} , and N_{n19}) in NMOD was basically consistent with that of points (N_{y7} , N_{y11} , N_{y15} , and N_{y19}) in NMODC (Figure 13a), but the volumetric water content in NMODC was slightly lower than that of corresponding points in NMOD. The main reason is that the points (N_{y7} , N_{y11} , N_{y15} , and N_{y19}) were located on both sides of the crack in NMODC, resulting in lateral infiltration into the crack to some extent.

In the middle layer, the points were located 0.4 m below the crack bottom; compared with the computational results of measuring points (N_{n8} , N_{n12} , N_{n16} , and N_{n20}) in NMOD, there was a local surge phenomenon in computational results of the measuring points (N_{y8} , N_{y12} , N_{y16} , and N_{y20}) in NMODC (Figure 13b) after the activation of the crack. The local surge phenomenon still existed at the lower points (Figure 13c) and the bottom points (Figure 13d); however, the increased amplitude of this surge decreased with the increasing depth of the measuring points.

In short, the volumetric water content of soil near the crack was considerably affected by simulated rainwater infiltration after the crack occurred, and the crack would be a potential threat to slope stability during rainfall.

5. Conclusions

In field test on slopes under local artificial rainfall, there are mainly two kinds of boundary constraints that affect test accuracy. The boundary constraints include the lateral infiltration and dissipation of rainwater, as well as the slope deformation retardation of non-rainfall areas to the rainfall area. We proposed a measure to address boundary constraints affecting test accuracy. The proposed measure is an isolated trench consisting of deep-buried isolated cloth at the local boundary. The isolated cloth should have characteristics of a dense texture, softness, good ductility, impermeability, and a smooth surface.

The local artificial rainfall test showed that the proposed measure effectively eliminated the deformation retardation outside the rainfall range, resulting in a through-crack parallel to the slope shoulder at the slope crest. An overall downward-cutting cracking form was realized.

The crack width developed slowly at first and then rapidly. As the crack occurred at the slope crest, rainwater infiltration aggravated the depthwise expansion. Based on rainfall tests and numerical simulations, it is worth noting that local sliding zone was formed in the upper part of the slope. The mechanism of the failure mode was due to a comprehensive effect, including rainwater flowing down along the cracks at the slope crest and the continuous infiltration at the slope surface.

In summation, a deep-buried isolated trench can solve the boundary constraints and provide an effective technical measure for the field slope test under artificial rainfall.

Author Contributions: L.W., analyses and writing; R.L. (Rongjian Li), analyses; S.Z., data; R.L. (Rongjin Li), data; W.B., field test; H.X., field test. All authors have read and agreed to the published version of the manuscript.

Funding: This research was supported by the National Natural Science Foundation of China (grant number 12102379), the Key R&D program of Shaanxi Province (2020ZDLGY07-03), and the China Geological Survey (DD20190268).

Institutional Review Board Statement: Not applicable.

Informed Consent Statement: Not applicable.

Data Availability Statement: The data presented in this study are all available in the article.

Conflicts of Interest: The authors declare no conflict of interest.

References

1. Duan, Z.; Zhao, F.S.; Chen, X.J. Types and spatio-temporal distribution of loess landslides in loess plateau region: A case study in Wuqi county. *J. Catastrophol.* **2011**, *26*, 52–56. (In Chinese)
2. Wang, T.; Zhao, X.L.; Qi, P.R. Impact of continued heavy rainfall on loess land slide hazard areas: A case study on Yan'an. *Geol. Surv. Res.* **2014**, *37*, 224–229. (In Chinese)
3. Sun, P.P.; Zhang, M.S.; Jiang, R.J.; Jia, J.; Liu, F.; Liu, M.M. Deformation and failure mechanism of rainfall-induced shallow loess landslide. *Geol. Bull. China* **2021**, *40*, 1617–1625. (In Chinese)
4. Peng, J.; Wang, S.; Wang, Q.; Zhuang, J.; Huang, W.; Zhu, X.; Leng, Y.; Ma, P. Distribution and genetic types of loess landslides in China. *J. Southeast Asian Earth Sci.* **2018**, *170*, 329–350. [[CrossRef](#)]
5. Gu, T.; Wang, J.; Lin, H.; Xue, Q.; Sun, B.; Kong, J.; Sun, J.; Wang, C.; Zhang, F.; Wang, X. The Spatiotemporal Relationship between Landslides and Mechanisms at the Heifangtai Terrace, Northwest China. *Water* **2021**, *13*, 3275. [[CrossRef](#)]
6. Huang, R.Q. Large-scale landslides and their sliding mechanisms in china since the 20th century. *Chin. J. Rock Mech. Eng.* **2007**, *26*, 433–454. (In Chinese)
7. Griffiths, D.V.; Marquez, R.M. Three-dimensional slope stability analysis by elasto-plastic finite elements. *Géotechnique* **2007**, *57*, 537–546. [[CrossRef](#)]
8. Ashraf, A.A.; Abdallah, S.B. Three-Dimensional Analysis of Seepage below and around Hydraulic Structures. *J. Hydrol. Eng.* **2009**, *14*, 243–247.
9. Hou, X.P.; Xu, Q.; Chen, S.H. An air element method for overflow boundary problem in seepage analysis. *Rock Soil Mech.* **2015**, *36*, 2345–2351. (In Chinese)
10. Li, G.R.; Chen, W.T.; Zhu, H.L.; Guo, Z.J.; Li, J.F.; Wang, T.; Hu, X.S. Influence of rain infiltration to stability of loess slope in the northeast Qinghai-Tibetan plateau. *Hydrogeol. Eng. Geol.* **2015**, *42*, 105–111. (In Chinese)

11. Lei, W.; Dong, H.; Chen, P.; Lv, H.; Fan, L.; Mei, G. Study on Runoff and Infiltration for Expansive Soil Slopes in Simulated Rainfall. *Water* **2020**, *12*, 222. [[CrossRef](#)]
12. Zhang, M.; Yang, L.; Ren, X.W.; Zhang, C.Y.; Zhang, T.L.; Zhang, J.J.; Shi, X.Y. Field model experiments to determine mechanisms of rainstorm-induced shallow landslides in the Feiyunjiang river basin. *Eng. Geol.* **2019**, *262*, 105348. [[CrossRef](#)]
13. Zhou, Z.; Fu, H.L.; Liu, B.C.; Tan, H.H.; Long, W.X.; Zhou, Y. In-situ monitoring test study on artificial rainfall infiltration of a well-instrumented accumulation slope. *China Railw. Sci.* **2006**, *27*, 11–15. (In Chinese)
14. Zhou, Z.; Fu, H.L.; Liu, B.C.; Tan, H.H.; Long, W.X. Artificial rainfall tests on a well-instrumented soil-rock-mixture slope. *Rock Soil Mech.* **2007**, *28*, 1391–1396. (In Chinese)
15. Fu, H.L.; Li, C.Y.; Guo, F.; Zhou, Z. Situ-test of abduction elements of landslide and its influence. *J. Cent. South Univ.* **2009**, *40*, 781–785. (In Chinese)
16. Tu, X.B.; Kwong, A.F.L.; Dai, F.C.; Tham, L.G.; Min, H. Field monitoring of rainfall infiltration in a loess slope and analysis of failure mechanism of rainfall-induced landslides. *Eng. Geol.* **2009**, *105*, 134–150. [[CrossRef](#)]
17. Zhang, M.S.; Li, T.L. Triggering factors and forming mechanism of loess landslides. *J. Eng. Geol.* **2011**, *19*, 530–540. (In Chinese)
18. Wang, G.; Sun, P.; Wu, L.Z.; Shi, L.Y.; Zhu, E.Z. Experimental study on mechanism of shallow loess landslides induced by rainfall. *J. Eng. Geol.* **2017**, *25*, 1252–1263. (In Chinese)
19. Liu, H.L.; Xu, Z.M.; Zhang, Y.; Wang, Z.Q. Evolutionary mechanism of slope fissures during rainfall and their affection slope stability: A case study of Dingjiafen landslide in Shuangbo country, Yunnan. *J. Catastrophol.* **2011**, *26*, 26–29. (In Chinese)
20. Xu, X.J.; Wang, L.B.; He, Z.J. Study of influence of vertical cracks on slope stability. *Yangtze River* **2009**, *40*, 46–48. (In Chinese)
21. Peng, J.B.; Wang, Q.Y.; Zhuang, J.Q.; Leng, Y.Q.; Fan, Z.J.; Wang, S.K. Dynamic formation mechanism of landslide disaster on the loess plateau. *J. Geomech.* **2020**, *26*, 714–730.
22. Ma, P.H.; Peng, J.B.; Zhu, X.H.; Tong, X.; Meng, Z.J.; Duan, Z. Regularities of rainfall infiltration in shallow loess. *Bull. Soil Water Conserv.* **2017**, *37*, 248–253. (In Chinese)
23. Miao, H.B.; Chai, S.F.; Wang, G.H. Influence factors for failure of cohesionless soil slopes triggered by heavy rainfall. *Chin. J. Geotech. Eng.* **2021**, *43*, 300–308. (In Chinese)
24. Sun, P.; Wang, H.; Wang, G.; Li, R.; Zhang, Z.; Huo, X. Field model experiments and numerical analysis of rainfall-induced shallow loess landslides. *Eng. Geol.* **2021**, *295*, 106411. [[CrossRef](#)]
25. Wen, Y.; Gao, P.; Mu, X.; Li, M.; Su, Y.; Wang, H. Experimental Study on Landslides in Terraced Fields in the Chinese Loessial Region under Extreme Rainfall. *Water* **2021**, *13*, 270. [[CrossRef](#)]
26. Yang, L.; Liu, E. Numerical Analysis of the Effects of Crack Characteristics on the Stress and Deformation of Unsaturated Soil Slopes. *Water* **2020**, *12*, 194. [[CrossRef](#)]
27. Sassa, K.; Hiroshi, F.; Wang, F.W.; Wang, G.H. *Progress in Landslide Science*; Springer: Berlin, Germany, 2007.
28. Liu, B.; Sun, S.L.; Liu, J.; Wang, E.X.; Chen, Y.Y. Fissure developed loess slope stability analysis under rainfall infiltration. *Geotech. Investig. Surv.* **2016**, *44*, 16–21. (In Chinese)
29. Yu, T.T.; Gu, S.P.; Shao, X.J.; He, H.X.; Cao, A.W. Stability analysis of reservoir bank slope considering tensile crack by the action of rainfall. *Yellow River* **2017**, *39*, 104–107. (In Chinese)
30. Liu, F.; Rui, Y.Q.; Zhang, C. Influence of tension cracks of slope crest on the stability of slope. *J. Liaoning Tech. Univ.* **2016**, *35*, 945–954. (In Chinese)
31. Geo-Slope International Ltd. *Slope/W for Slope Stability Analysis*; Geo-Slope International Ltd.: Calgary, AB, Canada, 2004.
32. Peng, G.Y.; Zhou, H.Q.; Ren, J.B.; Wu, R.Z. The influence of vertical fissures on land slope stability after rainfall. *J. Logist. Eng. Univ.* **2016**, *32*, 23–27. (In Chinese)
33. Elahe, J.; Philip, J.V.; Susan, C. S-D. The impact of evaporation induced cracks and precipitation on temporal slope stability. *Comput. Geotech.* **2020**, *122*, 103506.
34. Zhang, Y.H. Using equivalent penetration coefficient method to search the unconfined flow surface. *J. Eng. Geol.* **2004**, *12*, 187–192. (In Chinese)
35. Van Genuchten, M.T. A Closed-form Equation for Predicting the Hydraulic Conductivity of Unsaturated Soils. *Soil Sci. Soc. Am. J.* **1980**, *44*, 892–898. [[CrossRef](#)]